Contract No.:

This manuscript has been authored by Savannah River Nuclear Solutions (SRNS), LLC under Contract No. DE-AC09-08SR22470 with the U.S. Department of Energy (DOE) Office of Environmental Management (EM).

Spectroscopic Evidence of Uranium Immobilization in Acidic Wetlands by Natural Organic Matter and Plant Roots

Dien Li,*[,†] Daniel I. Kaplan,[†] Hyun-Shik Chang,[‡] John C. Seaman,[‡] Peter R. Jaffé,[∓] Paul Koster van Groos,[∓] Kirk G. Scheckel,[⊥] Carlo U. Segre,[#] Ning Chen,[$] De-Tong Jiang,[!!] Matthew Newville,[§] Antonio Lanzirotti[§]

[†] Savannah River National Laboratory, Aiken, South Carolina 29808, United States

[‡] Savannah River Ecology Laboratory, University of Georgia, Aiken, South Carolina 29802, United States

[∓] Department of Civil and Environmental Engineering, Princeton University, Princeton, New Jersey 08544, United States

[⊥] US Environmental Protection Agency, National Risk Management Research Laboratory Cincinnati, Ohio 45224, United States

[#] Physics Department & CSRRI, Illinois Institute of Technology, Chicago, Illinois 60616, United States

[$] Canadian Light Sources Inc., Saskatoon, Saskatchewan S7N 2V3, Canada

[!!] Department of Physics, University of Guelph, Guelph, Ontario N1G 2W1, Canada

[§] CARS, University of Chicago, Argonne, Illinois 60439, United States

ABSTRACT: Biogeochemistry of uranium in wetlands plays important roles in U immobilization in storage ponds of U mining and processing facilities, but has not been well understood. The objective of this work was to study molecular mechanisms responsible for high U retention by Savannah River Site (SRS) wetland sediments under varying redox and acidic (pH = 2.6-5.8) conditions using U L_3-edge X-ray absorption spectroscopy. Uranium in the SRS wetland sediments existed primarily as U(VI) bonded as a bidentate to carboxylic sites (U-C bond distance at ~2.88 Å), rather than phenolic or other sites of natural organic matter (NOM). In microcosms simulating the SRS wetland processes, U immobilization on roots was two orders of magnitude higher than on the adjacent brown or more distant white sands in which U was U(VI). Uranium on the roots were both U(IV) and U(VI), which were bonded as a bidentate to carbon, but the U(VI) may also form a U phosphate mineral. After 140 days of air exposure, all U(IV) was re-oxidized to U(VI), but remained as a bidentate bonding to carbon. This study demonstrated NOM and plant roots can highly immobilize U(VI) in the SRS acidic sediments, which has significant implication for the long-term stewardship of U-contaminated wetlands.

TOC:

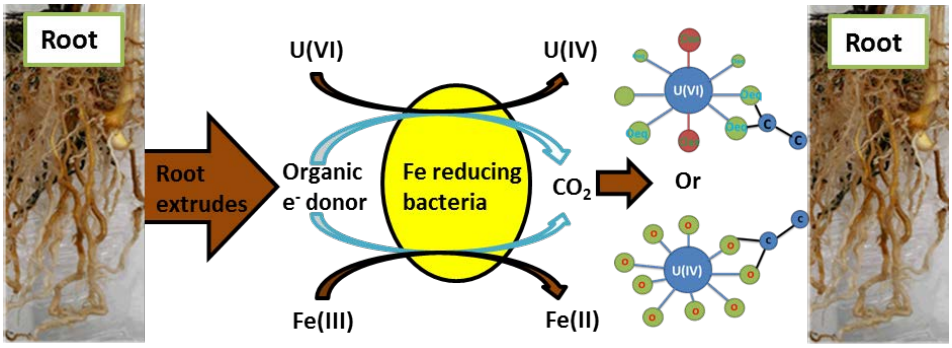

Keywords: Wetland sediments, uranium, molecular mechanisms, immobilization, spectroscopy

■ INTRODUCTION

There were several former U processing facilities at the Savannah River Site (SRS), Aiken, SC. As a result of their operations, uranium has entered the surrounding environments. For example, approximately 45,000 kg of depleted U in an acidic plume (pH 2.6-5.8) was released into the Tims Branch stream and its associated wetlands between 1958 and 1980.[1,2] Approximately 70% of this U still remains in the stream and its associated wetland sediments. Uranium is primarily in the U(VI) oxidation state,[1,2] and is strongly retained in the SRS wetland sediments,[2,3] mainly in association with acid exchangeable and organic matter fractions, and much less with Fe oxide fractions.[4] The U contaminated SRS wetlands, like storage ponds of U mining and processing facilities, are of great concern to the environment because they act as sinks and sources for continued U contamination. As such, potential remediation for the contaminated SRS sediments using apatite ($Ca_{10}(PO_4)_6(OH, F)_2$),[5-7] humic acid,[8] native trees,[9] natural hyper-accumulators,[10] and microbial metabolites[11] has been evaluated.

The biogeochemistry of U in wetlands (e.g., the SRS Tims Branch and its associated wetlands) is profoundly different than in uplands because of the presence of sharp geochemical gradients (e.g., pH, dissolved O_2, and E_h), active vegetation, elevated organic carbon concentrations and microbial activity, and the transient nature of hydraulic regimes (e.g., rainfall-induced flooding events and drought cycles). These conditions are related to the interface between relatively anoxic groundwater and oxic surface water, and are known to greatly affect the mobility of U and other redox sensitive metals. The development of remediation strategies for U contaminated sites has generally focused on the reduction of U(VI) to U(IV) through various biotic and abiotic processes.[12-29] However, reduced U can be readily re-oxidized to U(VI) and potentially be remobilized as wetlands undergo natural transient oxidizing events,[27,29-32] such

as seasonal drying or importation of large amounts of oxygenated rain and surface water. Thus, biotic and abiotic reduction of U may be questionable as an effective long-term U remediation technology for wetland systems.

Molecular mechanisms responsible for the strong retention of U in the oxidizing and acidic SRS wetlands are not sufficiently well understood, hindering our ability to make informed decisions related to the stewardship and management of the various SRS U-contaminated wetlands. Additional information is needed to facilitate development of risk assessment and remediation strategies for U contaminated SRS wetland sediments. From a broader perspective, natural and constructed wetlands have been used as a cost-effective means to immobilize U from mining and processing facilities.[33,34] While extensive U geochemical research has been conducted in neutral to alkaline environments dominated by strong U-complexing carbonates, very little research has been directed at understanding U immobilization in acidic (typically pH <5.5) wetland environments, and the extent that such information can be applied to natural wetlands is not known.

The objective of this work was to conduct spectroscopic measurements of wetland sediments and associated plant roots to help understand the biogeochemical factors responsible for the observed strong binding of U to the SRS wetland sediments. State-of-art analytical methods were used, including U L_3-edge X-ray absorption near-edge structure (XANES) and extended X-ray fine structure (EXAFS) spectroscopy, and X-ray fluorescence (XRF) mapping. Three sets of samples were investigated in this work. (1) U-contaminated SRS wetland sediments were studied to help understand U oxidation state and bonding environment under field conditions. (2) Non contaminated SRS sediments were amended with U(VI) over a range of pH values relevant to the SRS systems to provide additional information about the sensitivity of U binding and oxidation

state to pH changes. (3) Plant roots were recovered from a greenhouse microcosm study to provide a controlled system for studying the role of plant roots in U immobilization and U biogeochemistry.

■ MATERIALS AND METHODS

Contaminated SRS wetland sediment. The contaminated sediment was collected from the TNX-Area on the SRS. The TNX wetlands are located about 50 m from a research facility that released its wastes into a nearby basin and 500 m from the Savannah River. It is periodically flooded, depending on the river's seasonal water level. The specific location where the sample was collected was slightly elevated, and as such, was less likely to be flooded. The sample was collected after removing the top 10 cm of surface litter, and stored in its field-moist state in zip-lock bags at 5 ºC without taking precautions to eliminate air. The sediment had a pH of 4.5 in 1:1 soil and water ratio,[3,35] and contained 285 mg kg^{-1} U, 1427 mg kg^{-1} organic carbon and 900 mg kg^{-1} Fe oxides (Table S1 in Supporting Information). The sediment was composed of 53% sand, 22% silt and 19% clay; the clay was composed of kaolinite, illite, and hydroxy-interlayered-vermiculite, and goethite.[3,35] The desorption distribution coefficient (K_d) of U from this sediment was 1297 mL g^{-1}, consistent with values reported for other sediments from this site, ranging from 170 to 2110 mL g^{-1}.[35] Sequential extraction of this sediment indicated that the vast majority of the U was operationally defined as associated with the acid extractable fraction (36%) and the oxidizable organic matter fraction (37%), with relatively less associated with the reducible iron oxide fraction (9%) (Table S1 in Supporting Information).

Non-contaminated SRS wetland sediments with U sorption.[2] This sediment was collected about 50 m from the contaminated sediment. It was sampled at the same time and in a similar manner as described above for the contaminated sediment. The sediment contained three orders

of magnitude lower U (0.57 mg kg^{-1} U), 100 mg kg^{-1} Fe oxides and had similar pH (pH 4.2) and organic carbon content (1395 mg kg^{-1}) to the contaminated sediment (Table S1 in Supporting Information). In order to evaluate the impact of acidic pH conditions on U partitioning to wetland sediments, batch U sorption experiments were conducted using the non-contaminated sediments, with the experimental details provided in the Supporting Information. The batch sorption experiments confirmed that U was highly sorbed onto the non-contaminated SRS wetland sediment, with the sorption K_d values ranging from 384 to 19,974 mL g^{-1}. The U sorption onto the SRS wetland sediments appeared primarily associated with high content NOM, especially the acid exchangeable and organic fractions, in the sediments (Tables S1 and S2 in Supporting Information). The high U K_d values for these sediments indicate that U had been highly immobilized.[2] The residual sediment samples used in the batch experiments were recovered, air dried, and used for U L_3-edge XANES and EXAFS measurements, and XRF mapping.

SRS plant roots harvested from microcosms. Detailed microcosm experiments were described in our previous paper,[36] and a schematic diagram for the microcosm experimental setup was shown in Figure S1 (Supporting Information). In brief, water-washed Ottawa sand was added into cone-shaped pots with a 6.7 cm inner diameter. American bur-reeds (*Sparganium americanum*) transplanted from a non-contaminated SRS creek were grown under controlled temperature (25-30 ºC) and lighting (14 hours day^{-1}). An Fe(II)-rich nutrient solution containing 0.5 mmol L^{-1} Fe(II), 0.25 mmol L^{-1} PO_4^{3-}, and 1 mmol L^{-1} urea (no SO_4^{2-} or NO_3^-) was supplied for 73 days to keep the plants healthy while promoting Fe plaque formation on the roots under reducing conditions. After this initial 73-day period, a second nutrient solution containing no Fe(II), PO_4^{3-} or urea was supplied for 10 days to flush out residual Fe(II), organic carbon and

PO_4^{3-}. Between day 83 through 139, a third nutrient solution was introduced into the system that was composed of 20 µmol L^{-1} U(VI) (as uranyl acetate) amended to the second nutrient solution. The U(VI) nutrient solution reservoir was maintained in a glove bag filled with N_2 to minimize the introduction of oxygen. After completion of the microcosm experiments, the pots were dismantled, and plant roots were carefully harvested to minimize the loss of Fe (hydr)oxide plaque formed on the roots. This was accomplished by gently rinsing and soaking in water until essentially all the loose soil had been removed and only a red coating on the roots remained. Reddish brown sand samples near the roots and grayish white sand samples away from the roots were also collected. All the collected plant roots and sands were air dried in a circulating hood. No effort was made in the sample collection and handling protocol to minimize contact with air, but the sample drying, mounting (described below) and then storing into the capped containers were as quick as possible to minimize the change in redox chemistry. However, it is likely that some oxidation of the samples occurred during the collection, drying, and mounting process. The U L_3-edge XANES spectra of the sands and EXAFS spectra of the roots were collected 15 days after root harvest, and the EXAFS spectra of the two root samples were measured again 140 days after harvest to monitor the stability of U speciation in the samples after a protracted dry storage period. XRF maps of the roots were recorded 160 days after harvest.

U L_3-edge XANES and EXAFS measurement. Numerous studies have demonstrated that U L_3-edge XANES and EXAFS, and XRF mapping are valuable in understanding molecular mechanisms and chemical speciation of U in environmental samples.[15,16,27,37] In this study, U L_3-edge XANES and EXAFS spectra of all sediment and root samples were collected using the Hard X-ray Micro-Analysis beam line (HXMA or 06ID-1) at the Canadian Light Sources (CLS) [38], and then using the Materials Research Collaborative Access Team (MRCAT) Sector 10-BM

beamline at the Advanced Photon Source (APS) (Argonne National Lab, Argonne, IL).[39] To do so, 50-100 mg of each of the air-dried powder samples was pressed into a 6.3-mm diameter disk pellet, sealed by Kapton tape and stored in a capped container, which was done as quickly as possible to minimize redox chemistry changes.

The CLS HXMA beam line was configured to have Si (111) double crystal monochromators and Rh mirrors, detuned to 50% of peak intensity.[38] The monochromators were calibrated using the first inflection point at 17038 eV of the K-edge of yttrium metal foil that was mounted between two N_2-filled ionization chambers downstream of the sample. The U L_3-edge XANES and EXAFS spectra of all samples and uranyl acetate standard (Electron Microscopy Sciences, Hatfield, PA; mixed with silica powder to ~500 mg kg^{-1} U) were collected in fluorescence mode using a Canberra 32-element solid state Ge. The spectrum of UO_2 standard (Alfar Aesar, Ward Hill, MA) was collected using transmission mode. Eight layers of aluminum foil were placed in front of the Ge detector to reduce background Fe signals, in addition to a Sr-3 solid state filter used for other background signals that occur near the U L_3-edge. The storage ring was operated at 140-200 mA during the measurements. The U L_3-edge XANES and EXAFS spectra were recorded in the energy range of 17000-17800 eV at room temperature.

The MRCAT Sector 10-BM beam line used a double crystal water cooled Si (111) monochromator, detuned to 50% of peak intensity.[39] The APS storage ring was operated at 100 ± 5 mA during the measurements. Four layers of aluminum foil were used to eliminate Fe signals. The monochromators were calibrated using the first inflection point at 17038 eV of the K-edge of yttrium metal foil. The U L_3-edge XANES and EXAFS spectra were taken in fluorescence step-scanning mode using a Vortex 4-element silicon drift diode for energy discrimination, in the energy range of 17000-17750 eV at room temperature.

All the collected spectra were processed and analyzed using the IFEFFIT software package including Athena and Artemis.[40-42] Data from multiple scans were processed using Athena by aligning and merging the spectra followed by background subtraction using the AUTOBK algorithm. The U L_3-edge EXAFS data analysis was conducted on the merged and normalized spectra using Artemis.[16,37,43] Sodium uranyl triacetate (U-C),[44] chernikovite ($(H_3O)(UO_2)(PO_4)\bullet 3(H_2O)$) (U-P)[45] and a goethite cluster [46] with an assumed substitution of U for Fe (U-Fe) were used as structural models. Fits to the EXAFS data were made in R space (R from 1 to 3.2 Å) and obtained by taking the Fourier transform (FT) of $\chi(k)$ (k from 3 to 10.4 or 12). The simultaneous fitting was performed in R-space for individual or multiple data sets by using k weighting of 1, 2 and 3 for each data set to decrease the correlation between the best fit values for the local atomic uranyl structure (see Supporting Information).

X-ray fluorescence mapping and μ-XANES. Micro-XRF (μ-XRF) maps and micro-XANES (μ-XANES) spectra of selected sediments and two SRS plant roots harvested from microcosms were collected at Sector 13-ID-E (GeoSoilEnviroCARS) at the APS (Argonne National Laboratory, Argonne, IL), operating at 7 GeV (120 ± 5 mA) in top-up mode. Sector 13-ID used a liquid nitrogen cooled Si (111) double crystal monochromator that was calibrated using yttrium metal foil (17038 eV) and periodically verified during data collection to confirm stability. The samples were loaded into a Peltier-cooled cryostat system (-18 °C) on an x-y-θ stepping-motor stage to minimize beam-induced artifacts. μ-XRF maps (1×1 mm^2) of each sample were collected with 3 μm steps at 0.05 second integration for elemental distribution including U and Fe. U L_3-edge μ-XANES spectra of selected hot spots and other areas were collected from 17,000 to 17,500 eV using 0.4 eV steps within the main edge, and coarse (2-5 eV) steps over the pre-edge and post-edge regions. Fe K-edge μ-XANES data collection was

conducted in a similar fashion. The μ-XRF maps and μ-XANES spectra were collected in fluorescence mode using a Vortex-ME4 four-element silicon drift detector. Again, the collected μ-XANES spectra for U and Fe speciation of these samples were processed using the IFEFFIT software package.[40]

■ RESULTS AND DISCUSSION

Uranium in SRS Wetland Sediment. U L_3-edge EXAFS data of the SRS wetland sediment and its associated black NOM, and U sorbed non-contaminated SRS sediments at different pHs are shown in Figure 1A and 1B, respectively, where the symbols represent the Fourier transform EXAFS data, and the lines are the corresponding fits. The real part of Fourier transforms of two selected samples are shown in the insets. In Figure 1A, the peak at ~3 Å was consistent with the noise level, consequently fitting this peak to the U-Fe path failed. In Figure 1B, the peak at ~3 Å was absent for samples with U sorption at pH 2.8, but appeared to become stronger with an increase in pH, as observed for U adsorption profile onto goethite with pH,[8] which might indicate an increasing proportion of U that sorbed onto Fe (hydr)oxides in the SRS wetland sediments. However, the peak at ~3 Å was about or slightly above the noise level of the EXAFS data, and attempting to fit this peak to the U-Fe path significantly deteriorated the data fittings.

The corresponding EXAFS fitting parameters are given in Table 1. For the equatorial U-O_{eq} path, the fitted σ^2 values were similar to those found in U sorbed bone apatite materials [47,48] and humic substances,[49] but larger than those found in U sorbed biomass [37] and imogolite,[50]; nonetheless, the fitted coordination number (CN) values for the axial U-O_{ax} and equatorial U-O_{eq} were slightly larger than those reported in these reference materials. There was no evidence of U-U path or U mineral precipitates. The U-C path distance was 2.85 – 2.91 Å, indicating that U was bonded to C through two equatorial oxygen atoms as a bidentate species [37] rather than

monodentate species.[49,51,52] Uranium species in the SRS wetland sediments were dominated by uranyl that was bonding to NOM. Although the complex chemistry of NOM is not completely understood, various organic functional groups are present, among them phenolic OH, aromatic COOH, and aliphatic COOH are most dominant.[53] The relative proportions of these entities in the specific SRS wetland sediments used were not characterized. However, a previous study found that iodine was closely associated with aromatic or other aliphatic carboxylic acids, quinone-like structures (*e.g.*, NH_2), or a hemicellulose–lignin-like complex in the SRS wetland sediments.[54] U L_3-edge EXAFS data further indicated that U was preferentially bonding with the carboxylic group, rather than the phenolic OH group, in the NOM of the SRS wetland sediments.

U L_3-edge XANES spectra of a contaminated SRS wetland sediment (Figure S2A in Supporting Information), and U sorbed non-contaminated SRS sediment at pH 4.0 (Figure S2B) all overlap with the standard uranyl acetate spectrum, indicating that U in the SRS wetland sediments was U(VI). The Fe (Figure S2C) and U (Figure S2E) µ-XRF maps of the contaminated SRS wetland sediment demonstrated that Fe and U distributions were scattered, uncorrelated, and without significant hot spots, similar to Fe (Figure S2D) and U (Figure S2F) µ-XRF maps of the non-contaminated SRS wetland sediment with U sorbed at pH 4.0. These results indicated that U in the SRS wetland sediments might not be associated with secondary U mineral precipitates.

Uranium in SRS Plant Roots Harvested from Microcosms. U L_3-edge XANES spectra of two root samples collected from replicate microcosm pots, P5 and P6, as well as the associated brown (near the roots) and white (away from the roots) sands in microcosm pots are shown in Figure 2A and 2B, respectively. The spectra were collected on day 15 after root harvest. The spectra of brown and white sands were multiplied by 100 to ease peak identification. In Figure

2B, the inset picture shows the sampling locations of root P6 (spot a), brown (spot b) and white (spot c) sands. The spectrum of uranyl acetate (open circle) is also shown for comparison, which essentially overlaps the brown sand spectrum. For both P5 and P6 microcosm pots, the U concentrations in the roots were qualitatively >150 times higher than the concentration in the corresponding brown sands adjacent to the roots (<1 cm), and >300 times higher than the concentration in the white sands that were slightly farther from the roots (~2 cm), which indicated that U was primarily immobilized in close association with the roots rather than the sands. The U concentrations in samples from P6 microcosm pot were significantly higher than those in the corresponding samples from P5 microcosm pot, in agreement with chemical analysis of digested root and sand samples, and the higher abundance of *Geobacter*. *Spp.* in P6 microcosm pot.[36] The dominant species on the brown and white sands appeared to be the oxidized U(VI), while the chemical speciation of U on the roots will be described in more detail below.

The XANES spectra, $\chi(k)\times k^2$, and magnitude of Fourier transform of roots P5 and P6 collected on day 15 after harvest were presented in Figures 3A, 3C and 3E, respectively, and the real part of Fourier transform of root P6 was presented in the inset of Figure 3E. The XANES spectra of UO_2 (U(IV)) and uranyl acetate (U(VI)) were also included for comparison in Figure 3A, which shows that the XANES spectra of roots P5 and P6 were between the spectra of UO_2 and uranyl acetate. Linear combination fitting indicated that in root P5, 25% of U was U(IV), and 75% of U was U(VI); while in root P6, 38% of U was U(IV), and 62% of U was in U(VI). These results indicated that U species on roots included both U(IV) and U(VI), and that some of the influent U(VI) was reduced to U(IV) on the roots. The reduction of U(VI) to U(IV) might be related to the presence of iron-reducing bacteria, *Geobacter spp*. in the microcosm system. Their

273 population continuously increased after the introduction of the U(VI) acetate nutrient solution.[36]
274 It should also be noted that while attention was directed at storing and preparing the samples in a
275 manner that minimized contact with air, some U oxidation may have occurred as an experimental
276 artifact. In addition, the oxidation state of U species that was initially discharged to the
277 environment should have been U(VI) as a result of HNO_3 treatment as part of operations.

278 Similarly, the XANES spectra, $\chi(k)\times k^2$, and magnitude of Fourier transform of the same root
279 samples collected on day 140 after harvest were presented in Figures 3B, 3D and 3F,
280 respectively, and the real part of Fourier transform of root P6 was presented in the inset of Figure
281 3F. The XANES spectra of UO_2 (U(IV)) and uranyl acetate (U(VI)) were also included for
282 comparison in Figure 3B. The 140 day air dry was aimed at understanding the stability of the U
283 species on the plant roots under oxic conditions relevant to SRS seasonal drying processes. The
284 results shows that the XANES spectra of roots P5 and P6 overlapped the uranyl acetate
285 spectrum, and U species in both roots P5 and P6 were 100% U(VI). These results demonstrate
286 that the reduced U(IV) was re-oxidized to U(VI) after 140 days of exposure to air in Kapton-
287 sealed sample holders.[55] This observation was in agreement with a previous study that
288 demonstrated that at lower surface loading and under anoxic condition, the U(IV) sorbed onto
289 rutile was stable for at least 12 months, and the U(IV) sorbed on magnetite was stable for at least
290 4 months.[55]

291 The EXAFS fitting parameters for both roots P5 and P6, measured on days 15 and 140, are
292 summarized in Table 2. First, for both roots P5 and P6 after 15 days of their harvest, CN values
293 for U-O_{ax} path were 15-20% smaller, and CN values for U-O_{eq} path were 10-20% larger than the
294 corresponding CN values for the SRS contaminated wetland sediment in which U was 100%
295 U(VI). For both roots P5 and P6 after 140 days of their harvest, the CN values for U-O_{ax} and U-

296 O_{eq} paths were very similar to those for the SRS contaminated sediments (Table 1). These results
297 suggest that up to 20% of U in roots P5 and P6 15 days after harvest were in U(IV),[56] and all U
298 species in these two roots were in U(VI) after 140 days after harvest, qualitatively in agreement
299 with their XANES spectra. Second, for both roots P5 and P6, measured on day 15 or 140, the U-
300 C bond distances were 2.89 – 2.94 Å, with CN values of 1-2.3, indicating that U was bound to
301 carboxylic groups as a bidentate species. Third, there was a U-P path with its bond distance of
302 3.60 – 3.66 Å, and CN of 0.8 – 1.3, which indicated that some of the U on the roots was bonding
303 with P as a monodentate species. It is unclear whether the U species is bound to P associated
304 with the roots or microbes attached on the roots and/or secondary U-phosphate minerals.[12,22,47,48]
305 However, scanning electron microscopy images showed the presence of 3 – 6 µm particles on
306 root P6, U and P distributions on the roots, as indicated by their backscattering electron images,
307 were heterogeneous, but matching each other well,[36] These results may indicate the presence of a
308 U phosphate mineral precipitate, e.g., chernikovite ($(H_2O)_2(UO_2)_2(PO_4)_2$•$6H_2O$).[47] Fourth, there
309 was no clear evidence to indicate the presence of U-U path at ~4 Å (Figure 3E), which meant
310 that the U(IV) species present in roots P5 and P6 15 days after harvest was not in the form of
311 uraninite, but instead, more likely the reduced U(IV) was bonded with carboxylic groups in plant
312 roots.[13,14,22,55] Such a moderately labile U(IV) species found in the microcosm roots was directly
313 analogous to the so-called monomeric or non-uraninite U(IV), and can be readily oxidized to
314 U(VI) when exposed to air, as observed in the root spectra collected 140 days after harvest.
315 [13,14,22,55]

316 µ-XRF maps and µ-XANES spectra of roots P5 and P6 were collected 160 days after harvest.
317 Fe (Figure 4A) and U (Figure 4B) µ-XRF maps indicated that both Fe and U were
318 heterogeneously distributed on root P6, with specific Fe and U hot spots. These Fe and U

hotspots did not appear spatially correlated. Fe K-edge μ-XANES spectra of three marked hot spots were shown in Figure 4C, in comparison with the spectra of FeS, pyrite and goethite. The results indicated the presence of a Fe (hydr)oxide mineral and iron sulfide on root P6, in agreement with Fe and S backscattering electron distribution that demonstrated the presence of Fe sulfides on root P6.[36]. The iron sulfide was more likely pyrite, rather than FeS, and might be generated by the metabolism of sulfate-reducing bacteria. Although sulfate was not supplied in the nutrient solutions during the microcosm experiments, the pore fluid in the plant balls transplanted from the non-contaminated SRS creek contained 13.7 mg L^{-1} sulfate.[35] U L_3-edge μ-XANES spectra of three hot spots and one spot of low U counts are shown in Figure 4D, in comparison with the spectra of UO_2 and uranyl acetate, which demonstrated that U particles on root P6 were not uraninite, but a U(VI) mineral (e.g., uranyl phosphate minerals), in agreement with its bulk EXAFS analysis (Figure 3F and Table 2), and P and U backscattering electron distribution.[36]

Environmental Implications. Complex biogeochemical processes occurring in wetlands are strongly affected by plant and microbial activity. In the SRS wetland systems with limited phosphorus, plant roots and iron plaques commonly formed on roots can provide favorable conditions for Fe and possibly sulfate reducing bacteria to promote biotic U reduction. Both U(VI) and U(IV) species can be immobilized onto living plant roots as they are bound as a bidentate complex to carboxylic groups without the formation of either uraninite or uranyl phosphate minerals. The SRS typically experiences re-oxidizing conditions by seasonal wetting and drying, by periodical importation of large amounts of oxygenated precipitation, through which reduced U(IV) can be re-oxided to U(VI). U(VI) can also bind to carboxylic groups on NOM in wetlands as a bidentate complex. Therefore, even under acidic conditions where U(VI)

experiences limited absorption to sediment minerals, U(VI) can be fairly well immobilized by the high NOM content and living plant roots present in the SRS wetland sediments.

Uranium mining and processing wastes have been discharged to seepage or storage ponds that constitute natural or artificial wetlands. Among the key differences are that constructed wetlands are typically designed to remain flooded to promote non-fluctuating reducing conditions, and commonly use monoculture plants and soil amendments, such as various phosphate minerals, limestone, or gypsum ($CaSO_4$) to promote metal precipitation. Typical bio-reduction may not be effective in remediating U contamination in natural wetlands because the reduced U(IV) species can be easily re-oxidized when the wetlands become dry or receive a large amount of oxygenated surface or rain water. Other complex biogeochemical factors, such as groundwater chemistry, sediment mineralogy, vegetation, and microbial activity, can impact U immobilization in the wetlands. For example, U(VI) is fairly well immobilized by NOM and living plant roots in the wetlands. The U(VI) species may also be immobilized into U phosphate minerals when sufficient P is present in the systems. Understanding the molecular mechanisms of U retention in the wetland sediments can lead to a better assessment of its natural attenuation, immobilization and associated risks to the environment.

■ AUTHOR INFORMATION

Corresponding Author

*Phone: (803) 725 7520; fax: (803) 725 7673; E-mail: Dien.Li@srs.gov

■ ACKNOWLEDGMENTS

This work was supported by the Subsurface Biogeochemistry Research program within Department of Energy (DOE) Office of Sciences, Biological and Environmental Research. Work was conducted at Savanah River National Lab under the U.S. DOE Contract DE-AC09-96SR18500. Participation of Drs. J.C. Seaman and H.S. Chang in the current study was supported by the Savannah River Ecology Laboratory through a DOE Financial Assistance Award DE-FC09-07SR22506 to the University of Georgia Research Foundation. Work was conducted at Princeton University under the DOE Contract DE-SC0006847 and at University of Guelph supported by DTJ's NSERC Discovery Grant. Although Environmental Protection Agency (EPA) contributed to this article, the research presented was not directly performed or funded by EPA and was not subjected to EPA's quality system requirements. Consequently, the views, interpretations, and conclusions expressed in this article are solely those of the authors and do not necessarily reflect or represent EPA's views or policies. MRCAT operations are supported by the Department of Energy and the MRCAT member institutions. This research used resources of the Advanced Photon Source, a U.S. Department of Energy (DOE) Office of Science User Facility operated for the DOE Office of Science by Argonne National Laboratory under Contract No. DE-AC02-06CH11357. GeoSoilEnviroCARS (13-IDE) was supported by the NSF's Earth Sciences (EAR-0217473), DOE's Geosciences (DE-FG02-94ER14466), and the State of Illinois. Use of APS was supported by the U.S. DOE Office of Science, Office of Basic Energy Sciences, under contract No. W-31-109-ENG-38. Canadian Light Sources (CLS) was supported by the NSERC of Canada, the NRC of Canada, the Canadian Institutes of Health Research, and the Province of Saskatchewan.

SUPPORTING INFORMATION

The Supporting Information includes the details of batch sorption experiments and EXAFS data analysis, two tables, and one figure. Table S1 shows desorption K_d and sequential extraction data of U in the contaminated SRS wetland sediments; while Table S2 shows sorption K_d and sequential extraction data for U sorbed to non-contaminated SRS wetland sediments. Figure S1 shows a schematic diagram for the microcosm setup. Figure S2 shows U L_3-edge XANES spectra, Fe and U μ-XRF maps of the SRS contaminated wetland sediment and U sorbed to non-contaminated SRS wetland sediment. This information is available free of charge via the Internet at http://pubs.acs.org.

REFERENCES

(1) Bertsch, P. M.; Hunter, D. B.; Sutton, S. R.; Bajt, S.; Rivers, M. L. In-situe chemical speciation of uranium soils and sediments by micro-X-ray absorption spectroscopy. *Environ. Sci. Technol.* **1994**, *28*, 980-984.

(2) Li, D.; Seaman, J. C.; Chang, H. S.; Jaffe, P. R.; van Groos, P. K.; Jiang, D. T.; Chen, N.; Lin, J. R.; Arthur, Z.; Pan, Y. M.; Scheckel, K. G.; Newville, M.; Lanzirotti, A.; Kaplan, D. I. Retention and chemical speciation of uranium in an oxidized wetland sediment from the Savannah River Site. *J. Environ. Radioact.* **2014**, *131*, 40-46.

(3) Kaplan, D. I.; Serkiz, S. M. Quantification of thorium and uranium sorption to contaminated sediments. *J. Radioanal. Nucl. Chem.* **2001**, *248*, 529-535.

(4) Sowder, A. G.; Bertsch, P. M.; Morris, P. J. Partitioning and availability of uranium and nickel in contaminated riparian sediments. *J. Environ. Qual.* **2003**, *32*, 885-898.

(5) Arey, J. S.; Seaman, J. C.; Bertsch, P. M. Immobilization of uranium in contaminated sediments by hydroxyapatite addition. *Environ. Sci. Technol.* **1999**, *33*, 337-342.

(6) Seaman, J. C.; Arey, J. S.; Bertsch, P. M. Immobilization of nickel and other metals in contaminated sediments by hydroxyapatite addition. *J. Environ. Qual.* **2001**, *30*, 460-469.

(7) Kaplan, D. I.; Knox, A. S. Enhanced contaminant desorption induced by phosphate mineral additions to sediment. *Environ. Sci. Technol.* **2004**, *38*, 3153-3160.

(8) Wan, J. M.; Dong, W. M.; Tokunaga, T. K. Method to Attenuate U(VI) mobility in acidic waste plumes using humic acids. *Environ. Sci. Technol.* **2011**, *45*, 2331-2337.

(9) Hinton, T. G.; Knox, A. S.; Kaplan, D. I.; Sharitz, R. Phytoextraction of uranium and thorium by native trees in a contaminated wetland. *J. Radioanal. Nucl. Chem.* **2005**, *264*, 417-422.

(10) Knox, A. S.; Kaplan, D. I.; Hinton, T. G. Elevated uptake of Th and U by netted chain fern (Woodwardia areolata). *J. Radioanal. Nucl. Chem.* **2008**, *277*, 169-173.

(11) Turick, C. E.; Knox, A. S.; Leverette, C. L.; Kritzas, Y. G. In situ uranium stabilization by microbial metabolites. *J. Environ. Radioact.* **2008**, *99*, 890-899.

(12) Alessi, D. S.; Lezama-Pacheco, J. S.; Stubbs, J. E.; Janousch, M.; Bargar, J. R.; Persson, P.; Bernier-Latmani, R. The product of microbial uranium reduction includes multiple species with U(IV)-phosphate coordination. *Geochim. Cosmochim. Acta* **2014**, *131*, 115-127.

(13) Alessi, D. S.; Uster, B.; Veeramani, H.; Stubbs, J. E.; Lezama-Pacheco, J. S.; Bargar, J. R.; Bernier-Latmani, R. Method to estimate the contribution of molecular U(IV) to the product of U(VI) reduction. *Geochim. Cosmochim. Acta* **2010**, *74*, A11-A11.

(14) Alessi, D. S.; Uster, B.; Veeramani, H.; Suvorova, E. I.; Lezama-Pacheco, J. S.; Stubbs, J. E.; Bargar, J. R.; Bernier-Latmani, R. Quantitative separation of monomeric U(IV) from UO_2 in products of U(VI) reduction. *Environ. Sci. Technol.* **2012**, *46*, 6150-6157.

(15) Bargar, J. R.; Williams, K. H.; Campbell, K. M.; Long, P. E.; Stubbs, J. E.; Suvorova, E. I.; Lezama-Pacheco, J. S.; Alessi, D. S.; Stylo, M.; Webb, S. M.; Davis, J. A.; Giammar, D. E.; Blue, L. Y.; Bernier-Latmani, R. Uranium redox transition pathways in acetate-amended sediments. *Proc. Nat. Acad. Sci. USA* **2013**, *110*, 4506-4511.

(16) Kelly, S. D.; Kemner, K. M.; Carley, J.; Criddle, C.; Jardine, P. M.; Marsh, T. L.; Phillips, D.; Watson, D.; Wu, W. M. Speciation of uranium in sediments before and after in situ biostimulation. *Environ. Sci. Technol.* **2008**, *42*, 1558-1564.

(17) Law, G. T. W.; Geissler, A.; Burke, I. T.; Livens, F. R.; Lloyd, J. R.; McBeth, J. M.; Morris, K. Uranium redox cycling in sediment and biomineral systems. *Geomicrobiol. J.* **2011**, *28*, 497-506.

(18) Latta, D. E.; Boyanov, M. I.; Kemner, K. M.; O'Loughlin, E. J.; Scherer, M. M. Abiotic reduction of uranium by Fe(II) in soil. *Appl. Geochem.* **2012**, *27*, 1512-1524.

(19) O'Loughlin, E. J.; Kelly, S. D.; Kemner, K. M. XAFS Investigation of the interactions of U-VI with secondary mineralization products from the bioreduction of Fe-III oxides. *Environ. Sci. Technol.* **2010**, *44*, 1656-1661.

(20) Rui, X.; Kwon, M. J.; O'Loughlin, E. J.; Dunham-Cheatham, S.; Fein, J. B.; Bunker, B.; Kemner, K. M.; Boyanov, M. I. Bioreduction of hydrogen uranyl phosphate: Mechanisms and U(IV) products. *Environ. Sci. Technol.* **2013**, *47*, 5668-5678.

(21) Salome, K. R.; Green, S. J.; Beazley, M. J.; Webb, S. M.; Kostka, J. E.; Taillefert, M. The role of anaerobic respiration in the immobilization of uranium through biomineralization of phosphate minerals. *Geochim. Cosmochim. Acta* **2013**, *106*, 344-363.

(22) Sharp, J. O.; Lezama-Pacheco, J. S.; Schofield, E. J.; Junier, P.; Ulrich, K. U.; Chinni, S.; Veeramani, H.; Margot-Roquier, C.; Webb, S. M.; Tebo, B. M.; Giammar, D. E.; Bargar, J. R.; Bernier-Latmani, R. Uranium speciation and stability after reductive immobilization in aquifer sediments. *Geochim. Cosmochim. Acta* **2011**, *75*, 6497-6510.

(23) Sharp, J. O.; Schofield, E. J.; Veeramani, H.; Suvorova, E. I.; Kennedy, D. W.; Marshall, M. J.; Mehta, A.; Bargar, J. R.; Bernier-Latmani, R. Structural similarities between biogenic uraninites produced by phylogenetically and metabolically diverse bacteria. *Environ. Sci. Technol.* **2009**, *43*, 8295-8301.

(24) Stylo, M.; Alessi, D. S.; Shao, P. P.; Lezama-Pacheco, J. S.; Bargar, J. R.; Bernier-Latmani, R. Biogeochemical controls on the product of microbial U(VI) reduction. *Environ. Sci. Technol.* **2013**, *47*, 12351-12358.

(25) Suzuki, Y.; Kelly, S. D.; Kemner, K. M.; Banfield, J. F. Radionuclide contamination - Nanometre-size products of uranium bioreduction. *Nature* **2002**, *419*, 134-134.

(26) Tang, G. P.; Watson, D. B.; Wu, W. M.; Schadt, C. W.; Parker, J. C.; Brooks, S. C. U(VI) bioreduction with emulsified vegetable oil as the electron donor - model application to a field test. *Environ. Sci. Technol.* **2013**, *47*, 3218-3225.

(27) Tokunaga, T. K.; Wan, J. M.; Kim, Y. M.; Sutton, S. R.; Newville, M.; Lanzirotti, A.; Rao, W. Real-time X-ray absorption spectroscopy of uranium, iron, and manganese in contaminated sediments during bioreduction. *Environ. Sci. Technol.* **2008**, *42*, 2839-2844.

(28) Veeramani, H.; Scheinost, A. C.; Monsegue, N.; Qafoku, N. P.; Kukkadapu, R.; Newville, M.; Lanzirotti, A.; Pruden, A.; Murayama, M.; Hochella, M. F. Abiotic reductive immobilization of U(VI) by biogenic mackinawite. *Environ. Sci. Technol.* **2013**, *47*, 2361-2369.

(29) Wu, W. M.; Carley, J.; Luo, J.; Ginder-Vogel, M. A.; Cardenas, E.; Leigh, M. B.; Hwang, C. C.; Kelly, S. D.; Ruan, C. M.; Wu, L. Y.; Van Nostrand, J.; Gentry, T.; Lowe, K.; Mehlhorn, T.; Carroll, S.; Luo, W. S.; Fields, M. W.; Gu, B. H.; Watson, D.; Kemner, K. M.; Marsh, T.; Tiedje, J.; Zhou, J. Z.; Fendorf, S.; Kitanidis, P. K.; Jardine, P. M.; Criddle, C. S. In situ bioreduction of uranium (VI) to submicromolar levels and reoxidation by dissolved oxygen. *Environ. Sci. Technol.* **2007**, *41*, 5716-5723.

(30) Senko, J. M.; Kelly, S. D.; Dohnalkova, A. C.; McDonough, J. T.; Kemner, K. M.; Burgos, W. D. The effect of U(VI) bioreduction kinetics on subsequent reoxidation of biogenic U(IV). *Geochim. Cosmochim Acta* **2007**, *71*, 4644-4654.

(31) Wan, J. M.; Tokunaga, T. K.; Brodie, E.; Wang, Z. M.; Zheng, Z. P.; Herman, D.; Hazen, T. C.; Firestone, M. K.; Sutton, S. R. Reoxidation of bioreduced uranium under reducing conditions. *Environ. Sci. Technol.* **2005**, *39*, 6162-6169.

(32) Wilkins, M. J.; Livens, F. R.; Vaughan, D. J.; Beadle, I.; Lloyd, J. R. The influence of microbial redox cycling on radionuclide mobility in the subsurface at a low-level radioactive waste storage site. *Geobiol.* **2007**, *5*, 293-301.

(33) Noller, B. N.; Watters, R. A.; Woods, P. H. The role of biogeochemical processes in minimising uranium dispersion from a mine site. *J. Geochem. Explor.* **1997**, *58*, 37-50.

(34) Schoner, A.; Noubactep, C.; Buchel, G.; Sauter, M. Geochemistry of natural wetlands in former uranium milling sites (eastern Germany) and implications for uranium retention. *Chem. Erde-Geochem.* **2009**, *69*, 91-107.

(35) Kaplan, D. I.; Serkiz, S. M. *In-Situ Kd Values and Geochemical Behavior for Inorganic and Organic Constituents of Concern at the TNX Outfall Delta (U)*; Westinghouse Savannah River Company: Aiken, SC, 2000.

(36) Chang, H. S.; Buettner, S. W.; Seaman, J. C.; Jaffé, P. R.; Koster van Groos, P. G.; Li, D.; Peacock, A. D.; Scheckel, K. G.; Kaplan, D. I. Uranium immobilization in an iron-rich rhizosphere of a native wetland plant from the Savannah River Site under reducing conditions. *Environ. Sci. Technol.* **2014**, *48*, 9270-9278.

(37) Kelly, S. D.; Kemner, K. M.; Fein, J. B.; Fowle, D. A.; Boyanov, M. I.; Bunker, B. A.; Yee, N. X-ray absorption fine structure determination of pH-dependent U-bacterial cell wall interactions. *Geochim. Cosmochim. Acta* **2002**, *66*, 3855-3871.

(38) Jiang, D. T.; Chen, N.; Zhang, L.; Malgorzata, K.; Wright, G.; Igarashi, R.; Beauregard, D.; Kirkham, M.; McKibben, M.: XAFS at the Canadian Light Source. In *X-ray Absorption Fine Structure—XAFS13*; Hedman, B., Pianetta, P., Eds.; American Institute of Physics: 2007; pp 893-895.

(39) Kropf, A. J.; Katsoudas, J.; Chattopadhyay, S.; Shibata, T.; Lang, E. A.; Zyryanov, V. N.; Ravel, B.; McIvor, K.; Kemner, K. M.; Scheckel, K. G.; Bare, S. R.; Terry, J.; Kelly, S. D.; Bunker, B. A.; Segre, C. U. The new MRCAT (Sector 10) Bending Magnet beamline at the Advanced Photon Source. In *AIP Conference Proceedings*; 2010; pp 299-302.

(40) Ravel, B.; Newville, M. Athena, Artemis, Hephaestus: data analysis for X-ray absorption spectroscopy using IFEFFIT. *J. Synch. Rad.* **2005**, *12*, 537-541.

(41) Calvin, S. *XAFS for Everyone*; CRC Press: Boca Raton, FL, 2013.

(42) Kelly, S. D.: Uranium chemistry in soils and sediments. In *Development in Soil Sciences*; Elsevier: 2010; pp 411-465.

(43) Kelly, S. D.; Wu, W. M.; Yang, F.; Criddle, C. S.; Marsh, T. L.; O'Loughlin, E. J.; Ravel, B.; Watson, D.; Jardine, P. M.; Kemner, K. M. Uranium transformations in static microcosms. *Environ. Sci. Technol.* **2010**, *44*, 236-242.

(44) Templeton, D. H.; Zalkin, A.; Ruben, H.; Templeton, L. K. Redetermination and absolute configuration of sodium uranyl(VI) triacetate. *Acta Crystal. Sect. C-Cryst. Struct. Commun.* **1985**, *41*, 1439-1441.

(45) Morosin, B. Hydrogen uranyl phosphate tetrahydrate, a hydrogen-ion solid electrolyte. *Acta Crystal. Sect. B-Struct. Sci.* **1978**, *34*, 3732-3734.

(46) Gualtieri, A. F.; Venturelli, P. In situ study of the goethite-hematite phase transformation by real time synchrotron powder diffraction. *Am. Mineral.* **1999**, *84*, 895-904.

(47) Fuller, C. C.; Bargar, J. R.; Davis, J. A. Molecular-scale characterization of uranium sorption by bone apatite materials for a permeable reactive barrier demonstration. *Environ. Sci. Technol.* **2003**, *37*, 4642-4649.

(48) Fuller, C. C.; Bargar, J. R.; Davis, J. A.; Piana, M. J. Mechanisms of uranium interactions with hydroxyapatite: Implications for groundwater remediation. *Environ. Sci. Technol.* **2002**, *36*, 158-165.

(49) Schmeide, K.; Sachs, S.; Bubner, M.; Reich, T.; Heise, K. H.; Bernhard, G. Interaction of uranium(VI) with various modified and unmodified natural and synthetic humic substances studied by EXAFS and FTIR spectroscopy. *Inorg. Chim. Acta* **2003**, *351*, 133-140.

(50) Arai, Y.; McBeath, M.; Bargar, J. R.; Joye, J.; Davis, J. A.: Uranyl adsorption and surface speciation at the imogolite-water interface: Self-consistent spectroscopic and surface complexation models. *Geochim. Cosmochim. Acta* **2006**, *70*, 2492-2509.

(51) Denecke, M. A.; Pompe, S.; Reich, T.; Moll, H.; Bubner, M.; Heise, K. H.; Nicolai, R.; Nitsche, H. Measurements of the structural parameters for the interaction of uranium(VI) with natural and synthetic humic acids using EXAFS. *Radiochim. Acta* **1997**, *79*, 151-159.

(52) Denecke, M. A.; Reich, T.; Pompe, S.; Bubner, M.; Heise, K. H.; Nitsche, H.; Allen, P. G.; Bucher, J. J.; Edelstein, N. M.; Shuh, D. K.; Czerwinski, K. R. EXAFS investigations of the interaction of humic acids and model compounds with uranyl cations in solid complexes. *Radiochim. Acta* **1998**, *82*, 103-108.

(53) Sachs, S.; Bernhard, G. Influence of humic acids on the actinide migration in the environment: suitable humic acid model substances and their application in studies with uranium-a review. *J. Radioanal. Nucl. Chem.* **2011**, *290*, 17-29.

(54) Xu, C.; Zhong, J. Y.; Hatcher, P. G.; Zhang, S. J.; Li, H. P.; Ho, Y. F.; Schwehr, K. A.; Kaplan, D. I.; Roberts, K. A.; Brinkmeyer, R.; Yeager, C. M.; Santschi, P. H. Molecular environment of stable iodine and radioiodine (I-129) in natural organic matter: Evidence inferred from NMR and binding experiments at environmentally relevant concentrations. *Geochim. Cosmochim. Acta* **2012**, *97*, 166-182.

(55) Latta, D. E.; Mishra, B.; Cook, R. E.; Kemner, K. M.; Boyanov, M. I.: Stable U(IV) complexes form at high-affinity mineral surface sites. *Environ. Sci. Technol.* **2014**, *48*, 1683-1691.

(56) Cologgi, D. L.; Lampa-Pastirk, S.; Speers, A. M.; Kelly, S. D.; Reguera, G. Extracellular reduction of uranium via Geobacter conductive pili as a protective cellular mechanism. *Proc. Nat. Acad. Sci. USA* **2011**, *108*, 15248-15252.

562 **Table 1. EXAFS fitting data for uranium in the SRS wetland sediments.**

563

	Sample #	Paths	EXAFS parameters [a]					
			CN	R (Å)	σ^2 ($\times 10^{-3}$ Å^2)	E_0 (eV)	S_0^2	χ_v^2
Contaminated SRS sediment	#103	O_{ax}	2.3 ± 0.2	1.77 ± 0.01	2 ± 1	6.2	0.98	8.8
		O_{eq}	6.1 ± 1.2	2.36 ± 0.01	12 ± 3	6.2		
		C	1.1 ± 0.6	2.91 ± 0.01	3	6.2		
	NOM from #103	O_{ax}	2.2 ± 0.4	1.77 ± 0.01	2 ± 1	4.7	0.91	77
		O_{eq}	7.3 ± 3.0	2.37 ± 0.01	12 ± 5	4.7		
		C	1.8 ±1.5	2.86 ± 0.01	3	4.7		
U sorbed non-contaminated SRS sediments	#601 (pH = 2.8)	O_{ax}	2.3 ± 0.3	1.78 ± 0.01	3 ± 1	5.3	0.99	41
		O_{eq}	7.4 ± 2.0	2.38 ± 0.01	14 ± 4	5.3		
		C	2.2 ± 0.9	2.88 ± 0.01	3	5.3		
	#602 (pH = 3.6)	O_{ax}	2.3 ± 0.4	1.78 ± 0.01	2 ± 1	5.2	0.93	34
		O_{eq}	6.7 ± 2.0	2.38 ± 0.01	11 ± 4	5.2		
		C	1.3 ± 1.1	2.87 ± 0.01	3	5.2		
	#603 (pH = 4.0)	O_{ax}	2.2 ± 0.4	1.77 ± 0.01	1 ± 1	6.2	0.89	24
		O_{eq}	7.4 ± 2.7	2.38 ± 0.01	12 ± 5	6.2		
		C	1.7 ± 1.1	2.85 ± 0.01	3	6.2		
	#604 (pH = 5.2)	O_{ax}	2.2 ± 0.3	1.78 ± 0.01	1 ± 1	5.2	0.89	65
		O_{eq}	7.3 ± 2.7	2.38 ± 0.01	11 ± 3	5.2		
		C	1.4 ± 0.9	2.85 ± 0.01	3	5.2		
	#605 (pH = 6.2)	O_{ax}	2.2 ± 0.5	1.78 ± 0.01	3 ± 2	6.0	1.0	84
		O_{eq}	6.7 ± 3.0	2.36 ± 0.01	13 ± 6	6.0		
		C	1.1 ± 1.3	2.88 ± 0.01	3	6.0		

[a] CN - coordination number; R - bond distance; σ^2 - Debye-Waller factor; S_0^2 - amplitude reducing factor; χ_v^2 - reduced chi-square.

564

565

566 **Table 2. EXAFS fitting data of the SRS plant roots harvested from microcosms**

Root sample #		Paths	EXAFS parameters [a]					
			CN	R (Å)	σ^2 ($\times 10^{-3}$ Å^2)	E_0 (eV)	S_0^2	χ_v^2
P5	15 days	O_{ax}	1.9 ± 0.6	1.78 ± 0.01	2 ± 2	6.2	0.82	190
		O_{eq}	7.6 ± 3.9	2.35 ± 0.01	16 ± 8	6.2		
		C	2.3 ± 1.4	2.94 ± 0.01	1	6.2		
		P	0.9 ± 1.1	3.60 ± 0.04	3	6.2		
	140 days	O_{ax}	2.2 ± 0.1	1.79 ± 0.01	1 ± 1	6.8	0.95	2
		O_{eq}	7.2 ± 0.7	2.37 ± 0.01	14 ± 2	6.8		
		C	1.4 ± 0.4	2.89 ± 0.01	3	6.8		
		P	0.9 ± 0.4	3.65 ± 0.03	3	6.8		
P6	15 days	O_{ax}	1.9 ± 0.3	1.79 ± 0.01	2 ± 1	7.3	1.0	105
		O_{eq}	8.0 ± 1.3	2.35 ± 0.01	11 ± 4	7.3		
		C	1.0 ± 0.4	2.91 ± 0.01	1	7.3		
		P	0.8 ± 0.3	3.66 ± 0.03	3	7.3		
	140 days	O_{ax}	2.4 ± 0.2	1.78 ± 0.01	3 ± 1	5.8	0.95	11
		O_{eq}	6.7 ± 0.6	2.35 ± 0.01	13 ± 2	5.8		
		C	2.0 ± 0.4	2.89 ± 0.01	3	5.8		
		P	1.3 ± 0.3	3.62 ± 0.02	3	5.8		

[a] CN - coordination number; R - bond distance; σ^2 - Debye-Waller factor; S_0^2 - amplitude reducing factor; χ_v^2 - reduced chi-square.

567

568

569

570

571

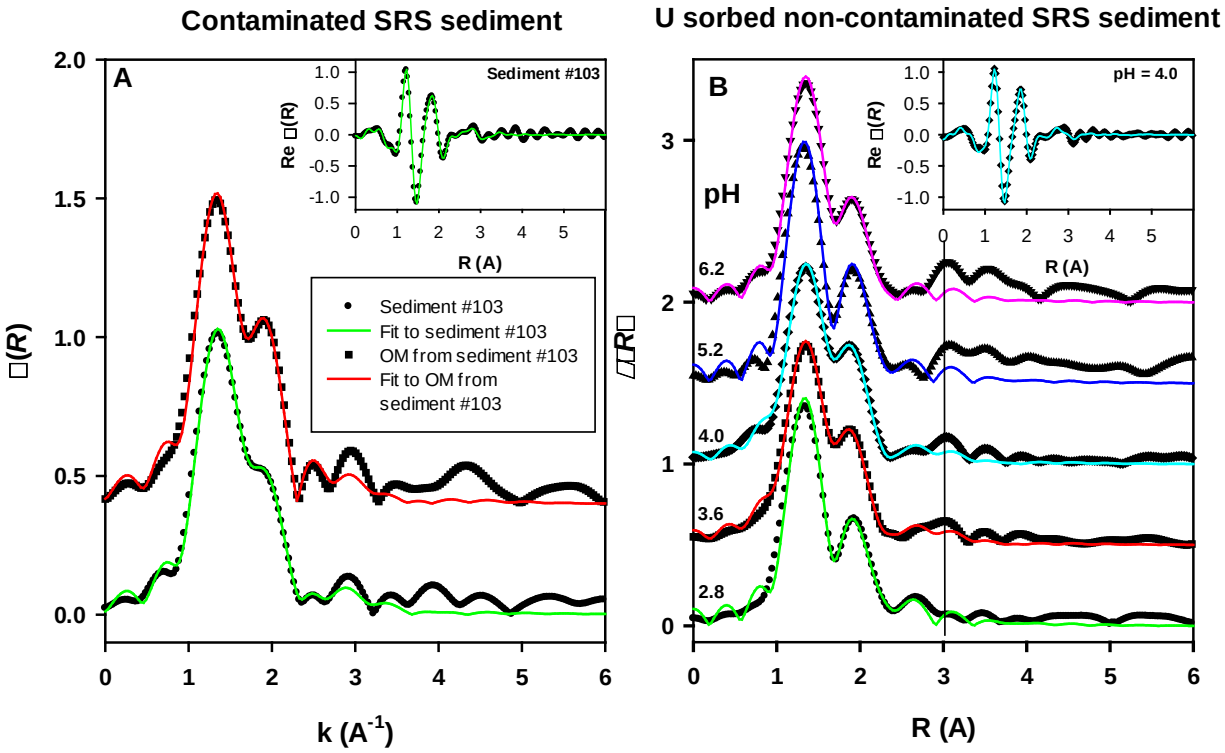

572

573

574 **Figure 1.** (A) Magnitude of Fourier transform of the SRS contaminated wetland sediment (<53
575 μm fraction) and its associcated black OM (ground to <53 μm), and (B) U sorbed to non-
576 contaminated SRS sediment at pH values relevant to the SRS sediments. Symbols represent
577 Fourier transform EXAFS data, and the lines are the corresponding fits. The real part of Fourier
578 transforms of two selected samples are shown in the insets.

579

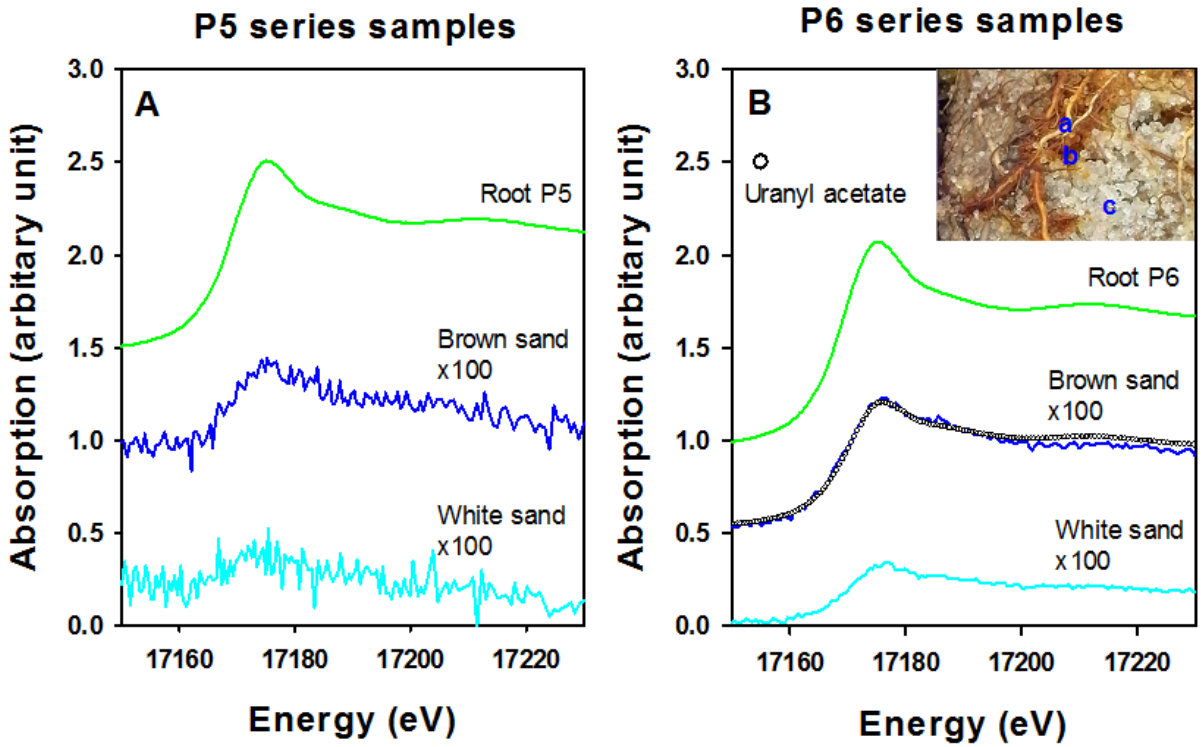

580

581

582 **Figure 2.** U L_3-edge XANES spectra of roots P5 (A) and P6 (B), as well as the associated brown
583 (near the roots) and white (away from the roots) sands in microcosm pots. The spectra of brown
584 and white sands were multiplied by 100. In Figure 1B, the inset is a picture showing the
585 sampling locations of root P6 (spot a), brown (spot b), and white (spot c) sands. Spectrum of
586 uranyl acetate (open circle) is also shown nearly overlapping the brown sand spectrum.

587

588

589

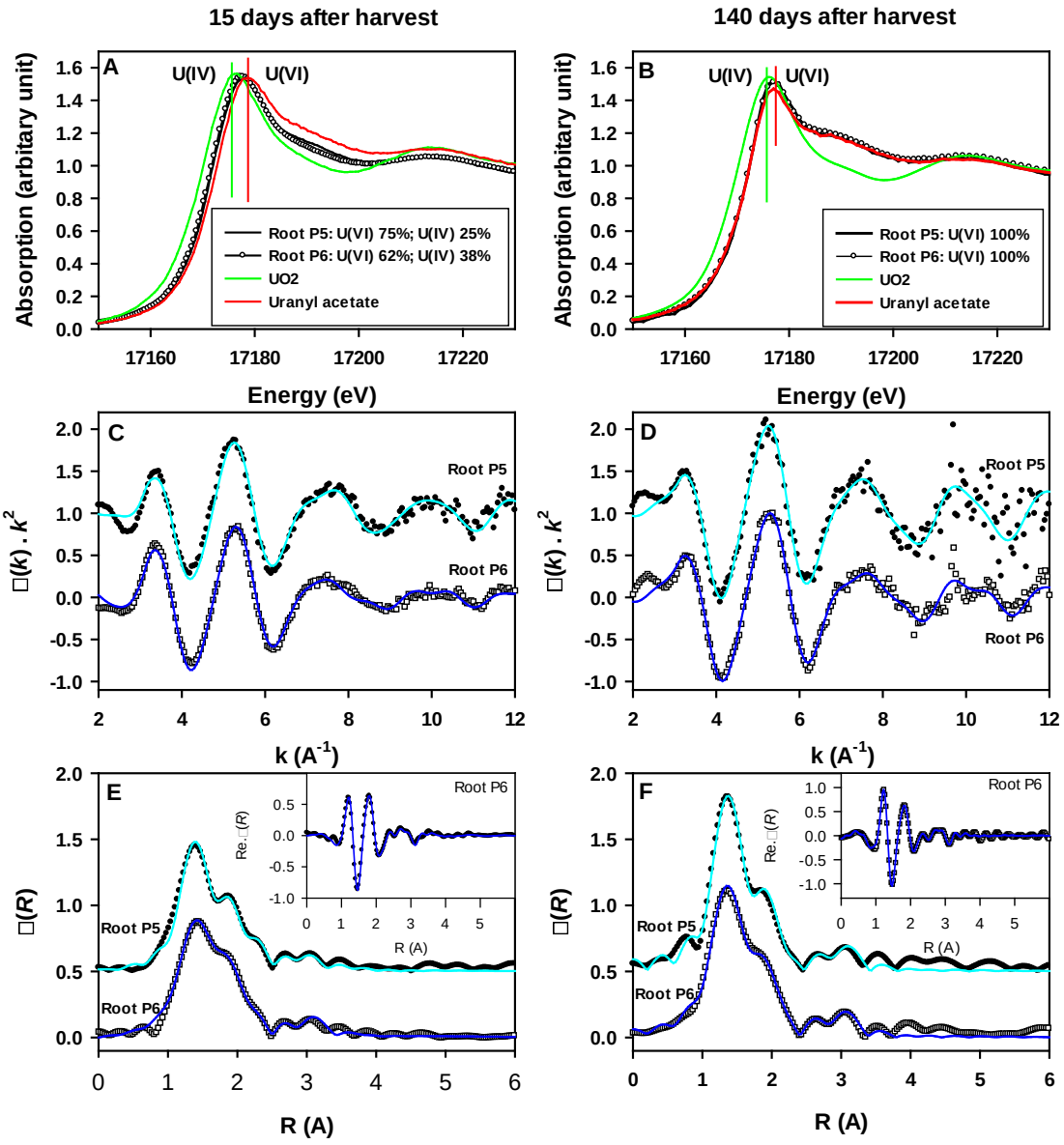

590

591

592 **Figure 3.** U L_3-edge XANES, and EXAFS data (symbol) and best fit model (line) of roots P5

593 and P6 measured on day 15 (A, C and E) and day 140 (B, D and F) after harvest. A and B: U L_3-

594 edge XANES spectra, C and D: $\chi(k) \times k^2$, E and F: magnitude of Fourier transform, with real

595 part of Fourier transform in the inset.

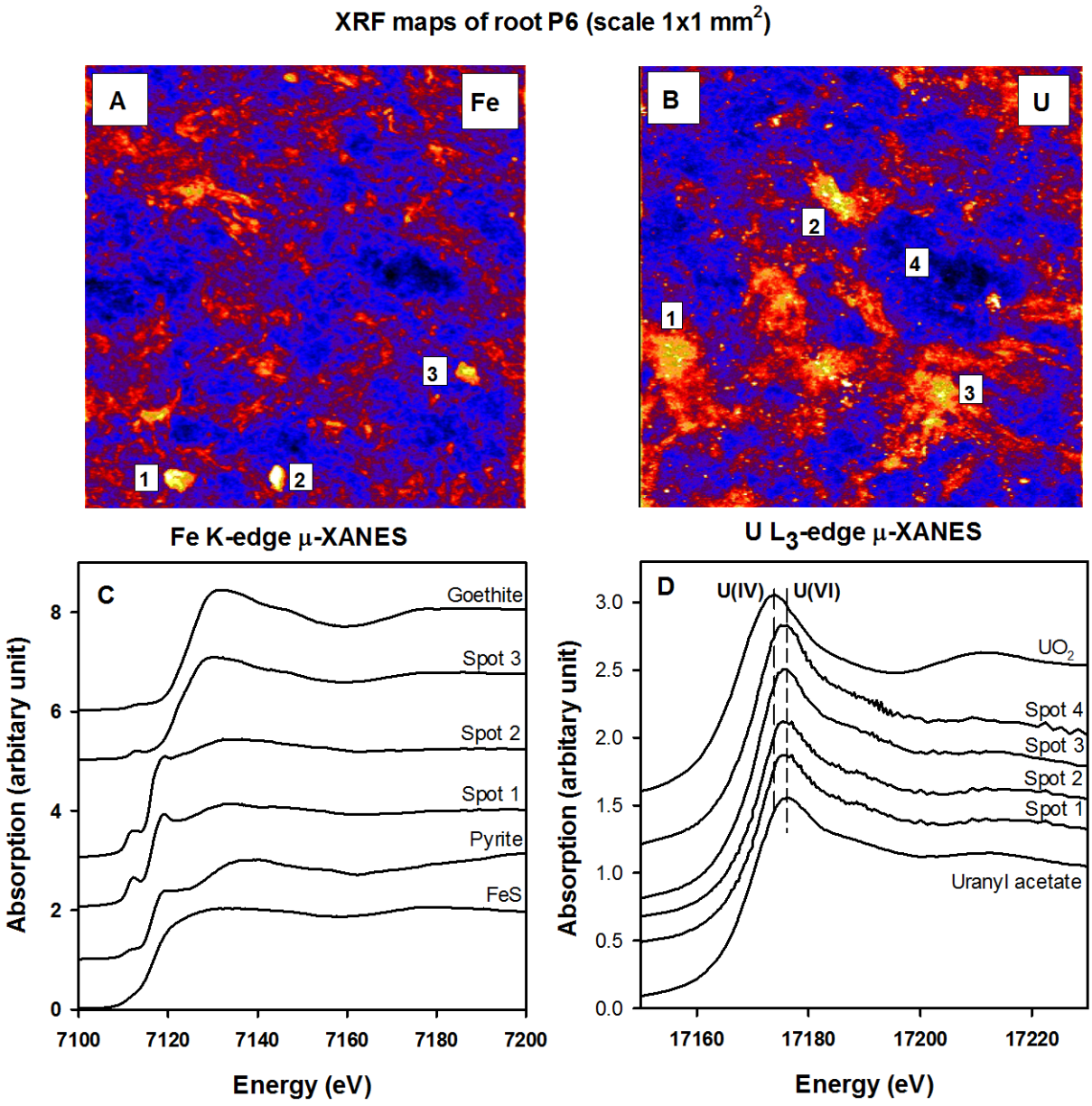

Figure 4. μ-XRF maps and μ-XANES spectra of root P6: (A) Fe μ-XRF map, (B) U μ-XRF map, (C) Fe K-edge μ-XANES spectra of three marked hot spots in comparison with the spectra of pyrite and goethite, and (D) U L_3-edge μ-XANES spectra of three hot spots and one spot of low U counts in comparison with the spectra of UO_2 and uranyl acetate.